LUNAR EXPLORATION FOR HE-3

Undergraduate Research Thesis
Submitted in partial fulfillment of the requirements for graduation
with research distinction in Earth Sciences
in the undergraduate colleges of
The Ohio State University

By

Bryan O'Reilly
The Ohio State University
2016

Approved by

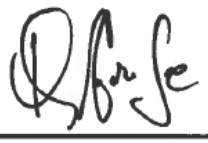

Professor Ralph R.B. von Frese, Project Advisor
School of Earth Sciences

TABLE OF CONTENTS

Abstract

As an essential component in the cleanest and most efficient form of fusion, Helium-3 (He-3) has the potential to produce incredible magnitudes of energy. However, naturally occurring He-3 only makes up 1.37 parts per million of He on Earth. The U.S. stockpile of He-3 has gradually decreased since 2001, with the price of He-3 jumping from $200 to $2,000 per liter. This reduced supply is largely due to the Department of Homeland Security's demand for neutron detection systems along our borders following the events of September 11th 2001. Lacking an atmosphere, the Moon's surface is only partial shielded from the solar wind that carries He-3 produced by fusion within the Sun. As the solar wind washes over the lunar surface, the He-3 embeds in the regolith. Analysis of Apollo samples suggests that the regolith holds a minimum He-3 concentration of about 20 ppb, which makes the regolith a viable source of He-3. Although satellite remote sensing cannot directly map this Helium isotope, it can map the distributions of titanium and volatiles, such as hydrogen, along with other components that act as proxies for concentrations of He-3. Using satellite data from the NASA's Lunar Prospector mission, two areas of considerable potential for holding large concentrations of He-3 were identified. Mare Tranquillitatis (8.5˚N 31.4˚E), for example, has the highest concentration of the Ti proxy that is indicative of high He-3 concentrations. This area also provides access to other elements such as iron, hydrogen and oxygen, which would be essential in any lunar mining mission. The South Pole Aitken basin also is of interest due to its large permanently shadowed areas that help to hold volatile He-3 and limit its migration due to diurnal heating.

ACKNOWLEDGMENTS

I would like to extend my deepest gratitude to my research advisor Dr. Ralph von Frese for his advice and guidance and Dr. Hyung Rae Kim for his time spent giving me valuable Matlab training. Additionally, I would like to thank Dr. Anne Carey for teaching me how to get the most out of a research experience and offering me advice throughout my undergraduate career, Dr. Daniel Pratt for helping to vastly enhance my technical and argumentative writing skills, and Dr. Berry Lyons for his mentorship. I'd also like to thank Erica Howat, Autumn Haagsma, and Amber Connor for their guidance at Battelle Memorial Institute in honing my ability to conduct and report professional research as well as offering valuable career advice. There have been many people who have helped me keep my sanity throughout my undergraduate career, for that I'd like to thank Kevin Inks, Patrick Burns, Avanti Krovi, Luke Lundy, Keegan Scott, and Claire Galasso. Many of my fellow students in the School of Earth Science have also contributed to the amazing time I've had at The Ohio State University, thank you to Andrew Burchwell, Mackenzie Scharenberg, Connor Gallagher, Tyler Rohan, Mario Gutierrez, and Laura Miller for helping me survive the sequence and field camp. Sigma Gamma Epsilon has been a large part of my academic career and so I'd also like to thank all of our officers including Brian Ares, Ally Brady, and Adrien van Wagenen. Finally, I'd like to thank the newer generation of geoscientist that I met as I finished my last year: Nick Rodgers, Taylor Hollis, my coworker Judith Straathof, and special thanks to Shelby Brewster. NASA provided a large portion of the instrumental data used. The Ohio State University College of Arts and Sciences Division of Natural and Mathematical Sciences through the Mayers Summer Research Scholarship and the Shell Exploration and Production Company funded this research.

LIST OF FIGURES

INTRODUCTION

Helium-3 (He-3) is a helium ion with a single neutron that is becoming exceedingly rare and expensive to access on Earth. Naturally occurring He-3 makes up an estimated 1.37 parts per million of all He on Earth (Shea and Morgan, 2010). The only reliable way to produce a sufficient amount of He-3 for the skyrocketing demand is through the decay of tritium or hydrogen-3, the radioactive isotope used in nuclear warheads. Thus, the demand for tritium determines the rate of He-3 production. As a result, the rapid consumption of the United States' He-3 stockpile has caused a large increase in demand over the past decade (e.g., Shea and Morgan, 2010). In 2001, for example, the United Stated government held roughly 235,000 liters of He-3 that had been reduced to 50,000 liters by 2010. Figure 1 illustrates the dramatic decrease in He-3 supply that caused the price of He-3 to jump from about $200 per liter to $2,000 per liter.

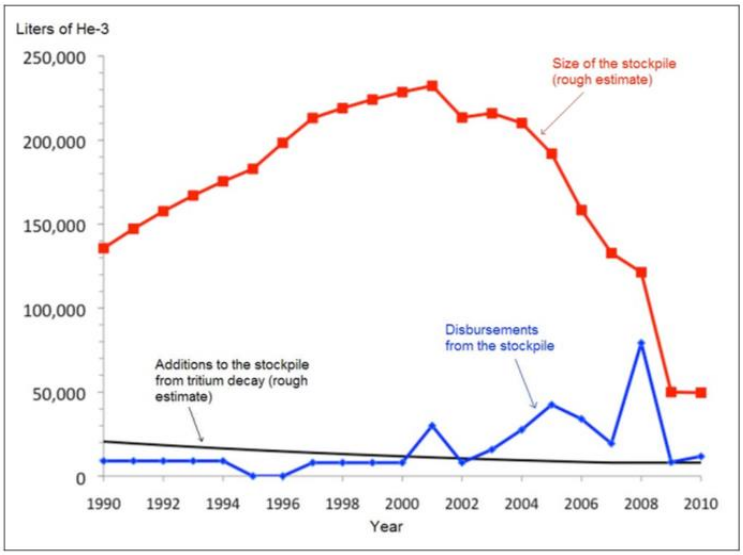

Figure 1. The history of the He-3 supply of the US from 1990 to 2010 in terms of the stockpile's size in liters (redline), disbursement rate, and estimated growth (black line) through tritium decay (Shea and Morgan, 2010).

The driving force behind the increase in He-3 demand is its use since 9/11/2001 by the Departments of National and Homeland Security in neutron detection devices. In this context, neutron detection devices are used to prevent the smuggling of radioactive material across the US border. These devices are also used to monitor the security of specialized nuclear weapons sites to ensure the continued safe storage of dangerous radioactive materials. The oil and gas industry also uses He-3 to power neutron detection devices for well logging applications. These instruments help detect the presence of hydrocarbons within geologic formations (e.g., Nikitin and Bliven, 2010).

In addition to neutron detection, He-3 is used in cryogenics research and the medical industry. He-3 is critical for low-temperature research because it can stably maintain temperatures below 0.8° Kelvin. In quantum mechanics research, He-3 facilities observing particles as environments reach temperatures within a millikelvin of absolute zero. Quantum computing and nanoscience also require cryogenic temperatures fueled by helium-3 (Cho, 2009). The evolving shortage in the He-3 supply inhibits low-temperature physics research, and could also render useless billions of dollars of scientific infrastructure investment. The operation of facilities like the Japan Proton Accelerator Research Complex, for example, which require the sensitivity that He-3 neutron detectors offer to produce usable data, are becoming severely limited by the current He-3 shortage. Medical applications where He-3 is inhaled and polarized to provide MRI scans of the lungs also are being increasing affected by growing He-3 shortage.

Another possible use of He-3 is to produce energy from the helium-3 deuterium (D) fusion reaction. This fusion reaction produces much cleaner energy than that produced by fission or other fusion processes. This fusion reaction also is more practical to implement than deuterium-deuterium (D-D) or tritium-deuterium (T-D) fusion reactions that require a magnetic

containment field to concentrate the elements in extremely high temperatures. However, the He-3-D reaction only requires an electrostatic containment field making the process much simpler and more feasible to implement (Mahdavi and Kaleji, 2009). This fusion reaction also produces a free proton that can be converted directly into energy far beyond that available from the steam-powered generator. He-3 is aneutronic, meaning the He-3 D fusion process only produces around 3-4 radioactive neutrons (Mahdavi and Kaleji, 2009). Thus, the He-3-D reaction requires significantly less shielding due to the lack of radioactive byproducts. Decreasing the amount of shielding together with the increased energy output also makes the reaction a viable fuel for spaceships (Ashley et al., 2000). The successful implementation of this fusion process would completely revolutionize the energy industry and space exploration.

Clearly, an alternate supply of He-3 must be found to meet current and future demands. Naturally occurring He-3 is produced by fusion reactions within the Sun and transported into the rest of the solar system via solar plasma winds. Our magnetosphere shields Earth from the winds so that extremely low quantities of He-3 are found on the planet. However, the Moon lacks a magnetic field so that its surface undergoes partial exposure to solar winds. This exposure results in the deposition of He-3 within the lunar regolith. Apollo samples and remote satellite sensing studies of the lunar surface suggest that the regolith maintains an average He-3 concentration of ~20ppb (Johnson et al., 1999).

Several factors determine where He-3 is concentrated within the lunar regolith. The Moon's orbit around the Earth and across its magnetotail, for example, variably exposes the lunar surface to solar winds. When the Moon is on the far side of Earth relative to the Sun, it rests within the Earth's magnetotail, and thus is shielded from the solar plasmas. When the Moon is in between the Sun and Earth, on the other hand, the far side is completely exposed to solar

winds. Other factors differentially concentrating He-3 within the lunar regolith include the solar wind's interactions with crustal magnetic anomalies and changes of topographic relief. Lunar He-3 exploration also must consider the distribution of proxies like titanium dioxide (TiO_2) that, on the Moon, tends to appear as ilmenite ($FeTiO_3$). Ilmenite in particular correlates with He-3 concentrations up to 100 times greater than do olivine, pyroxene, plagioclase and other TiO_2-free minerals (Fa and Ya-Qiu, 2007).

These factors are used to establish exploration strategies for locating lunar He-3 deposits. Higher concentrations of He-3, for example, are expected for the minimally shielded lunar far side. In addition, equatorial latitudes that experience increased solar wind exposure may host enhanced He-3 concentrations compared to the lunar poles. Ilmenite forms in igneous and metamorphic environments, thus making impact basins as prospects of particular interest. Impact basins also undergo extreme temperature and pressure changes that further promote the formation of this important mineral (Schmitt 2006).

Schmitt (2006) summarized initial research on the exploration for lunar He-3 that identified potential areas of high He-3 concentration. Mare Tranquillitatis, for example, is considered a particularly attractive site for a manned lunar base and the mining of lunar He-3. This site also holds Fe, Ti, and other minerals important for cost-effective, on-site production of construction materials and O_2 from mineralized oxygen. In siting a manned lunar base, water may be extracted atomically bound OH^- and lunar ice, and other issues that need to be addressed in choosing a manned lunar base.

The present research study further tests the recommended locations (e.g. Mare Tranquillitatis) of high He-3 concentrations. In particular, the utility of satellite-based Gamma Ray Spectrometers (GRS) is investigated to indirectly map He-3 abundances in terms of the

surficial abundances of gamma-radiating elements like titanium, oxygen and iron that reflect distributions of lunar ilmenite (e.g., Hasebe et al., 2008). In addition, satellite microwave measurements may be used to estimate regolith thickness, maturity, and dielectric constants to help map out He-3 concentrations and other lunar mineral deposits (Wang, 2010).

Satellite remote sensing data from past lunar missions are used to estimate TiO_2 and hydrogen concentrations, and the solar wind flux over the crust to identify lunar He-3 prospects. These results may help constrain the fiscal and technological viability of mining lunar He-3.

Current uses of helium-3 far outpace its supply and production on Earth. This shortage is detrimental to areas ranging from national security to important physics and medical research. The growing decrease of He-3 stores also drastically limits efforts to make He-3-D fusion a realistic energy source. However, the growing demand may well be satisfied with the He-3 concentrations hosted within the regolith of our closest celestial neighbor, the Moon. Indeed, the mining of He-3 on the Moon is an imminent, if not the next, giant leap for space exploration (Schmitt, 2006).

Elements of this research were presented at the fall'15 Undergraduate Student Poster Forum and the spring'16 Denman Undergraduate Research Forum of The Ohio State University. Further aspects of this research were presented at the annual conferences of the Geologic Society of America (O'Reilly and von Frese, 2015) and NASA's Lunar and Planetary Institute (O'Reilly and von Frese, 2016).

METHODS

National Aeronautics and Space Administration (NASA) data collection

The elemental abundance data for this research were collected from NASA's publicly available Planetary Data System (PDS) Geoscience Node. Specifically, the data were observed by the Lunar Prospector (LP) mission's gamma ray and neutron spectrometer tools and processed by the LP Spectrometer Team as part of a NASA Lunar Data Analysis Program. Elemental abundances of Ti were derived from LP gamma ray spectrometer (Feldman et al., 1999) observations acquired during the high-altitude portion of the LP mission. For the Ti distribution, the data are given in units of elemental weight percent (Prettyman et al., 2002). The half-degree hydrogen abundances came from the LP neutron spectrometer epithermal neutron data that had been corrected by the thermal neutron data (Feldman et al., 2001). Equations 3 and 4 of Feldman et al. (2001) show how the corrected epithermal data were converted into hydrogen abundances as parts per million (ppm). Note, however, that these abundances can be unreliable in regions of high thorium and rare-Earth element abundances (Maurice et al., 2004).

In general, using the above method yields an average ±1.7 wt% uncertainty in the TiO_2 estimates (Elphic et al., 2002). Estimates from areas with higher levels of TiO_2 are considered to be more reliable than those from lower TiO_2 areas. Uncertainties in H estimates are typically less than 1% over latitudes ±70° and increase significantly towards the poles (Feldman et al., 2001). Estimates of H taken from large lunar craters in the South Pole showed uncertainties averaging around 50% (Feldman et al., 2001).

Modeling

The raw elemental abundance data were converted from the original ASCII files to Microsoft Excel through the "paste special" tool for import into MATLAB. Once imported, the data were processed by the scripts in Appendix A to produce various lunar abundance maps. The

script in Figure A1 produces contour maps of the elemental data on the lunar near and far sides using the M_Map MATLAB mapping package (Pawlowicz 2014). This script uses the sinusoidal map projection to produce equal-area representations of the abundance data.

The script in Figure A2 produces stereographic projections of abundances in the lunar polar regions. Equation 1 (Fa and Ya-Qiu, 2007) was used to estimate crustal exposure to solar wind flux as a percentage in terms of lunar longitude (θ) and latitude (Φ) in degrees, and the constant flux (F_0) at a subsolar point. Here, f represents the amount of time the lunar surface is fully shielded from solar winds by Earth's magnetotail in the span of 28 days (one orbital period). To produce the normalized solar wind flux, the model assumed $F_0 = 0.5$, and f = 0.25 based on the amount of time the moon is in the magnetotail. Equation 1 was implemented by the MATLAB script in Figure A3 to produce a contour map (Figure 2) of the lunar near and far side exposures in percent of the maximum solar wind flux over a single lunar orbital period. These maps in the sinusoidal map projection were obtained using the previously cited M_map mapping package.

$$\textbf{1)}\quad \boldsymbol{F(\Phi,\theta) = F_0 cos(\Phi) * \begin{cases} 2 + sin(\theta - f\pi) - sin(\theta + f\pi), |\theta| \le \pi(.5 - f) \\ 1 + sin(|\theta| - f\pi), \pi(0.5 - f) \le |\theta| \le \pi(.5 + f) \\ 2, \pi(.5 + f) \le |\theta| \le \pi \end{cases}}$$

RESULTS

Solar Flux

Figure 2 shows that the Moon's orbit around Earth largely affects the intensity of solar exposure on its surface, with the near side receiving significantly lower exposure than the far side. This is due to Earth's magnetosphere which, during a full Moon when the near side is facing the Sun, rests within Earth's magnetotail shielded from solar radiation.

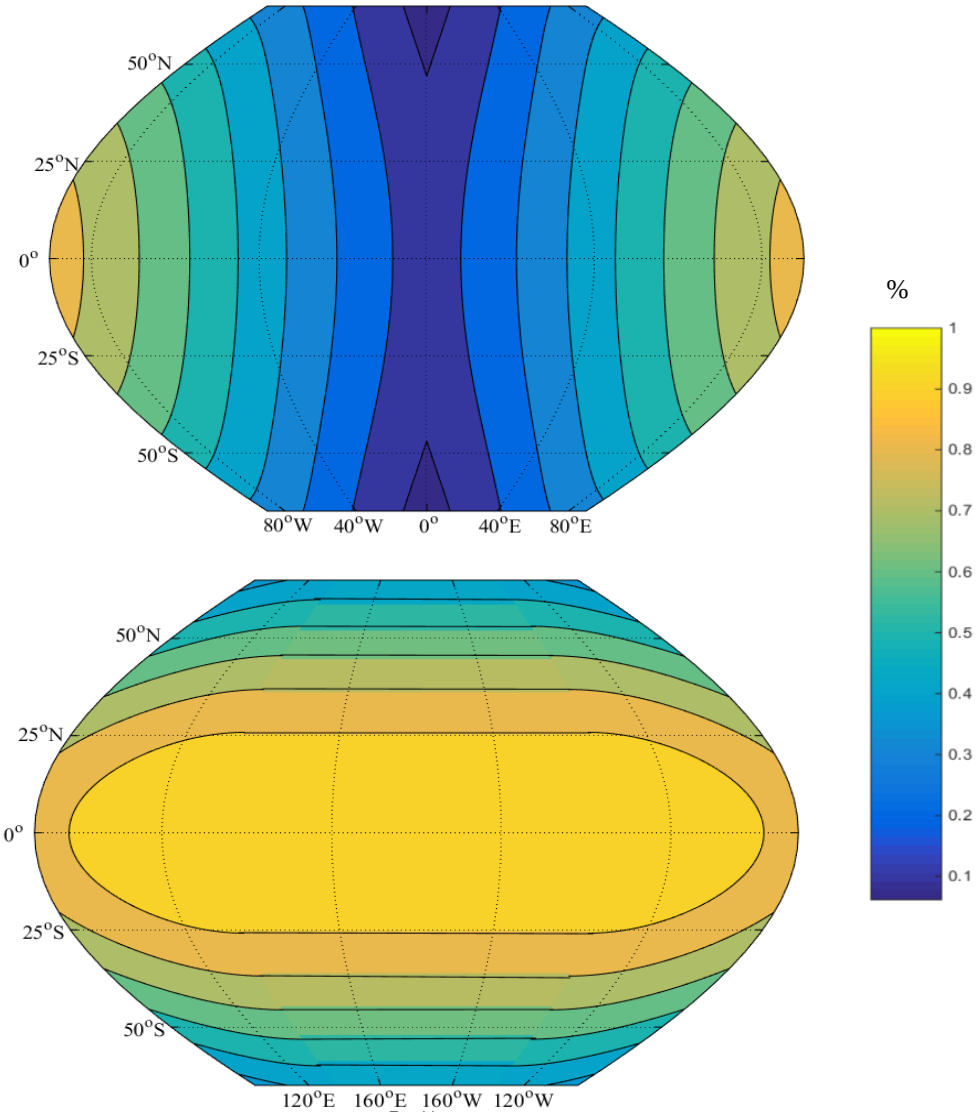

Figure 2. Solar flux as a percent of solar wind flux exposure per lunar cycle for the near (top) and far (bottom) sides of the lunar surface between 65°S - 65°N.

Titanium Distribution

The distribution of Ti correlates with large impact events (Schmitt, 2006), and thus the highest Ti concentrations are within the maria of the lunar near side (Figure 3). Mare Tranquillitatis, in particular, appears to have the highest overall concentration. On the moon, Ti occurs as the mineral ilmenite ($FeTiO_3$) with the crystal structure that locks in the small He-3 atoms. The blank strip surrounding 180°E in Figure 3 reflects a no-data area due to lack of orbital coverage by the satellite (Feldman et al., 1999).

Diurnal Heating

Areas within ±60˚ latitudes experience large average daily temperature shifts. The Apollo 15 site (26.13224 N, 3.63400 E), for example, underwent a shift from 374˚K to 92˚K (Heiken et al., 1991). The areas around the poles typically stay within 10˚ of 115˚K with even smaller variations in permanently shadowed craters (Vasavada et al., 1999). Volatiles are essentially baked out of the regolith when subjected to these extreme temperature changes (Cocks, 2010).

Polar Migration

After volatiles are released from the lunar regolith, they are either redeposited on the lunar surface or released into space (Cocks 2010). Figure 4 shows the increase of hydrogen around the poles compared to lower longitudes. This measurable increase is attributed to permanently shadowed craters, which prevent massive temperature fluctuations and provide shielding from micrometeoroids. The blank strips surrounding 180°E in Figure 4 reflect areas with no data due to lack of orbital coverage by the satellite (Feldman et al., 1999).

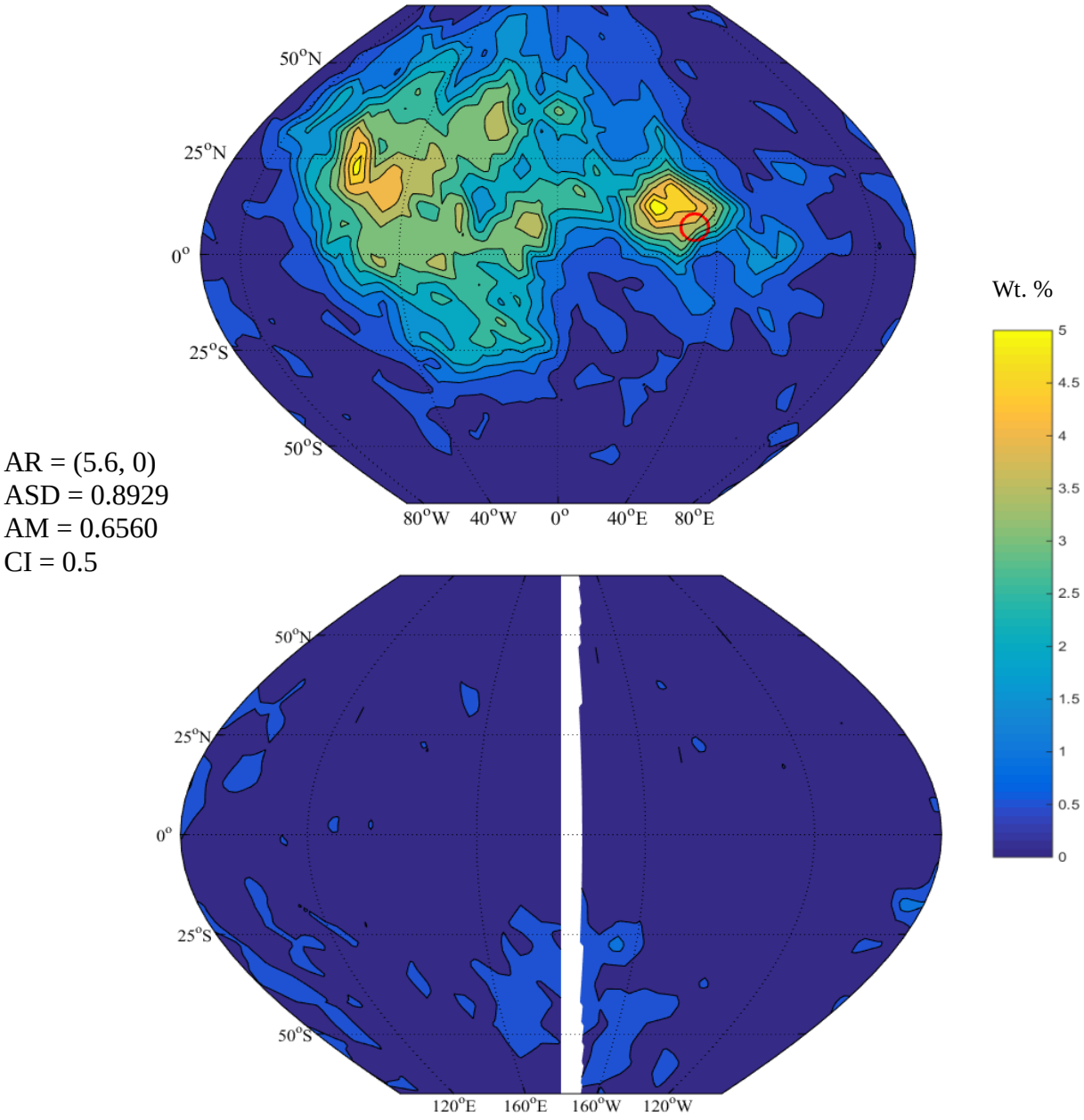

Figure 3. Weight percent Ti distribution for the near (top) and far (bottom) sides of the lunar surface from 65°S - 65°N. Mare Tranquillitatis is highlighted (8.5°N, 31.4°E) as an area of high Ti. Map statistics include the amplitude range (AR) of (max, min) values, amplitude standard deviation (ASD), amplitude mean (AM), and contour interval (CI) in weight %.

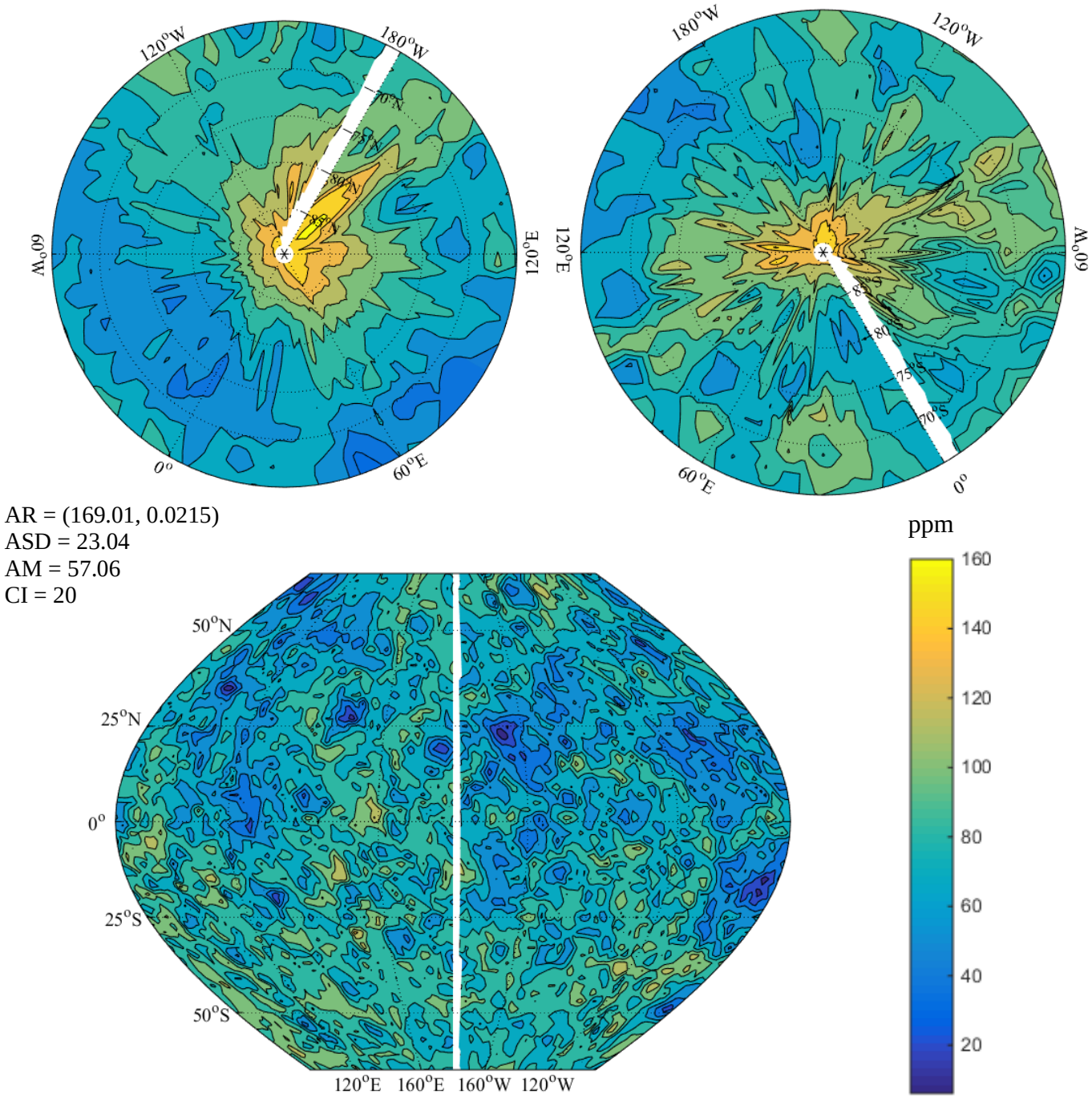

Figure 4. Volatile hydrogen concentrations in ppm for the lunar north pole (top left) from 90°N - 65°N, south pole (top right) from 90°S - 65°S, and the far side (bottom) from 90°W - 90°E and from 65°S - 65°N of the lunar surface. Map statistics include amplitude range (AR) of (max, min) values, amplitude standard deviation (ASD), amplitude mean (AM), and contour interval (CI) in ppm.

DISCUSSION

The data above contain implications for the search for large concentrations of He-3. The only method for deposition of He-3 is through exposure of the regolith to solar radiation carrying the isotope. Figure 5 shows the geometry of the Moon's exposure to solar radiation over a single orbital period (28 days). Accordingly, most of this exposure occurs on the far side of the Moon when it is between the Sun and Earth outside the magnetosphere.

In general, the areas of high solar exposure are also subject to extreme diurnal

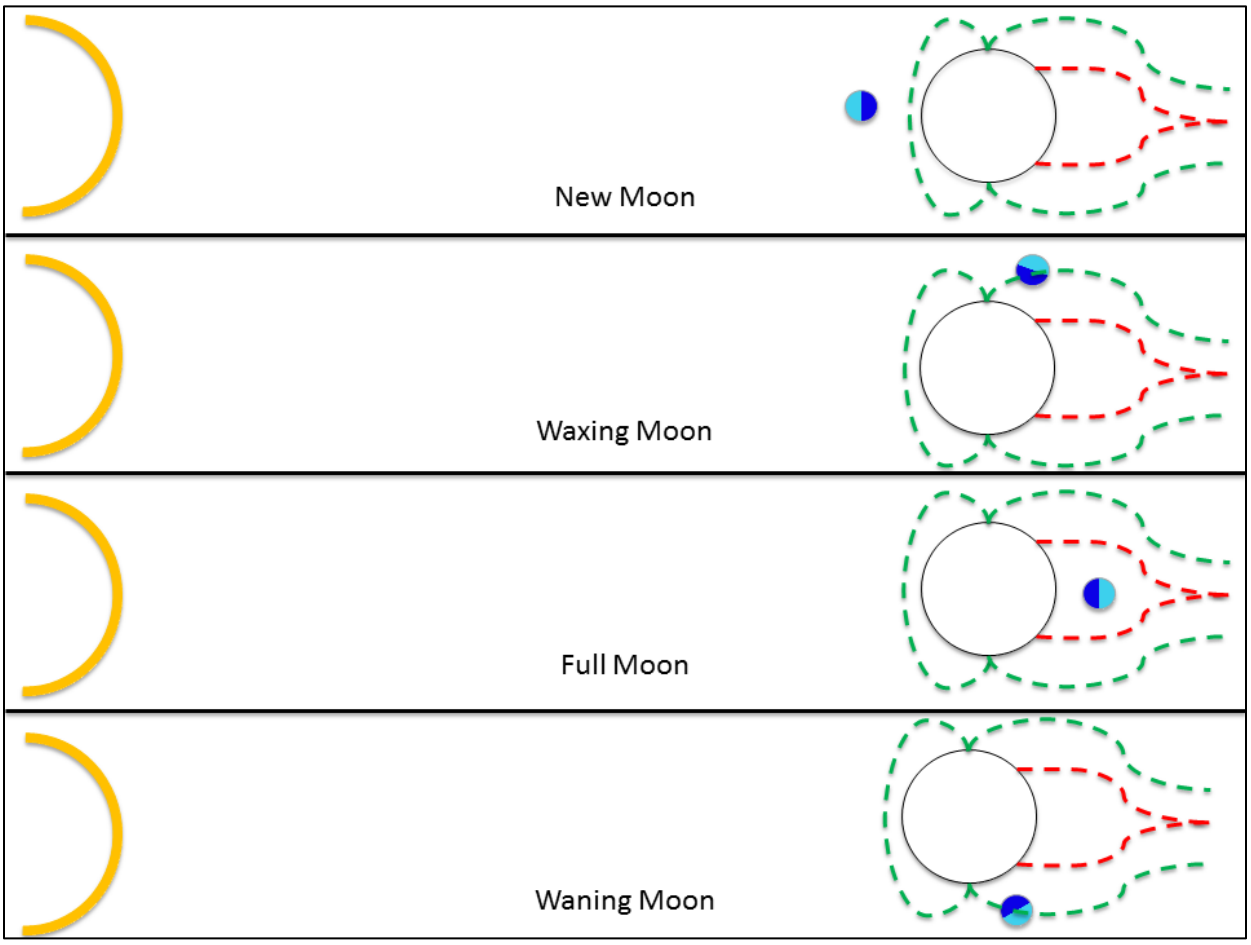

Figure 5. A 2-D geometric rendering of the relationship between the Sun (orange), Earth (large circle), and the moon (small circle) throughout a lunar orbital period. The moon is positioned outside the magnetosphere (green dashed line) during a new moon exposing the far side (light blue). The moon is positioned inside the protective magnetotail (red dashed line) during a full moon preventing exposure of the near side (dark blue).

temperature fluctuations. During the lunar orbital period, these drastic temperature changes will occur due to the prolonged exposure or protection from solar radiation causing the deposited volatiles to leave the regolith and possibly be re-ionized and –deposited onto the lunar surface (Cocks, 2010). This implies that many of the volatiles initially deposited by solar wind exposure do not remain stably in place. The distribution of hydrogen measured in Figure 4 suggests that the volatiles in general may be concentrated around the poles.

Much like hydrogen, He-3 is also deposited in the regolith through solar wind. However, exposing these elements to extreme temperature shifts causes them to vaporize and leave the lunar surface. Some of these volatiles are re-ionized due to subsequent solar wind exposure and possibly deposited again near the poles where they are better protected from temperature changes (Cocks, 2010). This mechanism could help explain the larger polar accumulations of volatiles.

The lunar polar regions offer protection from extreme temperature variations, which also may be provided by the presence of permanently shadowed craters. These craters not only protect volatiles from vaporizing out of the regolith, but they also shield the regolith from micrometeorite impacts that disturb the surface encouraging the further release of volatiles. These polar regions are estimated by the Lunar Prospector team (Schmitt, 2000) to contain roughly 5 to 15 times more hydrogen. Figure 6 shows an example of the permanently shadowed Shackleton crater.

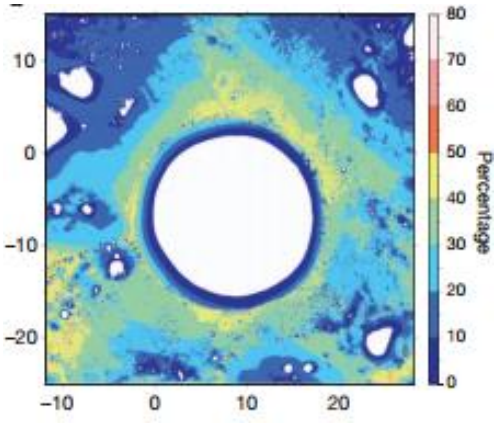

Figure 6. The Shackleton crater located near the South Pole, where the colors indicate the percentage of time illuminated during a single lunar orbital period. The rim of the crater contains zero (white) and near zero illumination values which identify it as a permanently shadowed crater (Zuber et al., 2012).

Another important aspect to consider is the relationship between titanium (Ti) and He-3. The majority of Ti on the Moon appears in the form of ilmenite ($FeTiO_3$). Tests done on lunar ilmenite, olivine, pyroxene, and plagioclase show that for grains in the same size range from the same soil, ilmenite ($FeTiO_3$) contains 10 to 100 more times as much He-3 (Fa and Ya-Qiu, 2007). The structure of ilmenite, seen in Figure 7, is better able to hold onto the small He-3 ions when subjected to extreme conditions. This suggests that He-3 is more protected from the effects of massive temperature shifts than other volatiles when high concentrations of Ti are present. Figure 3 shows that most of the Ti on the Moon appears in the large impact craters of the nearside.

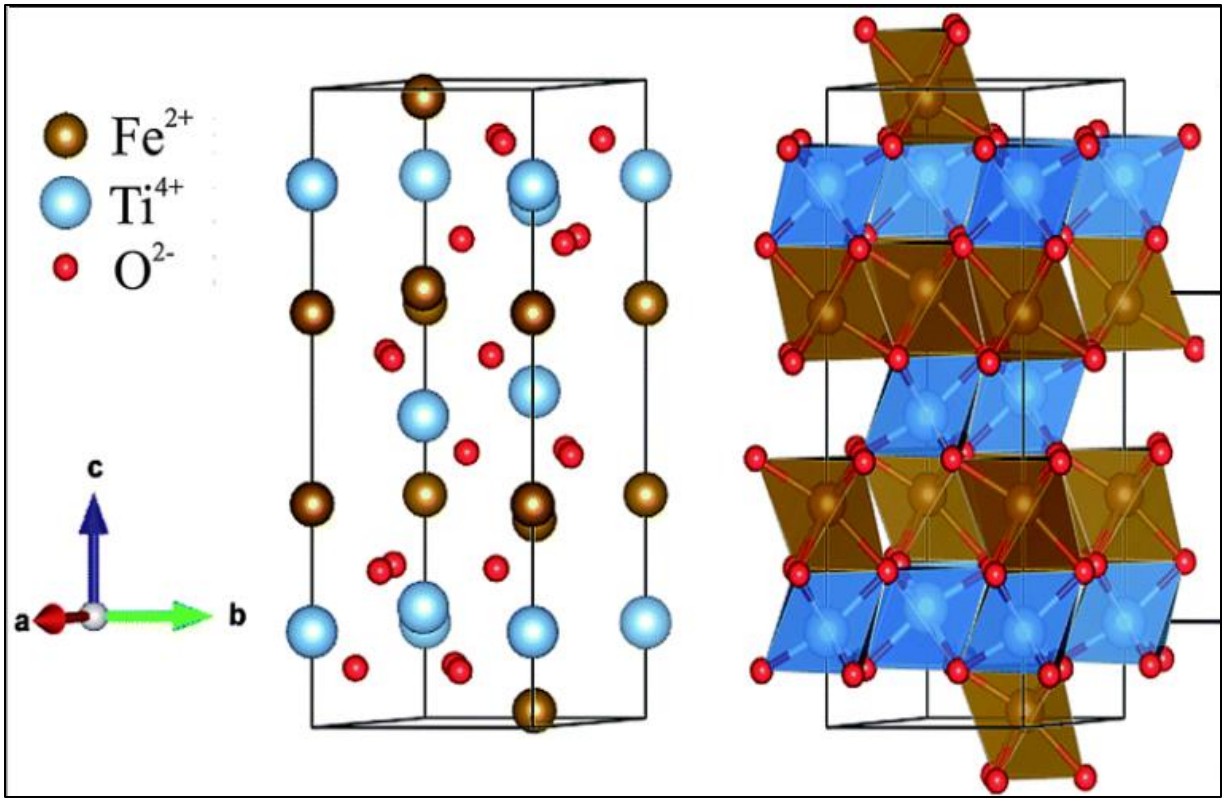

Figure 7. The crystal structure of Ilmenite. The alternating layers of Fe and Ti along with the rhombohedral shape shown above allow for tighter confinement of loose He-3 ions (Ribeiro and Lazaro, 2014).

With all of these factors considered, two areas of particular interest are suggested for holding large concentrations of He-3. They include Mare Tranquillitatis (8.5˚N 31.4˚E) that has the highest concentration of Ti on the lunar surface, and thus also possible large He-3 stores. The second area of interest is the South Pole Aitken basin with large permanently shadowed craters that enhance its ability to hold volatiles like He-3 through diurnal heating shifts over the lunar orbital period. These permanently shadowed craters would protect the volatiles from temperature shifts and the regolith from being disturbed by micrometeorite impacts.

CONCLUSIONS

Lunar resource development is an extensive and expensive effort, however, this study seeks to introduce the need to explore for these resources. This study examined the shortage of available He-3 and the affected industries. Hopes in the distant future for clean fusion energy also rest on access to this valuable resource. As U.S. stockpiles diminish and demand continues, the economic incentive for the acquisition of He-3 deposits on the moon becomes an increasingly attractive option.

The objective of this study was to use available satellite data to estimate possible locations of large lunar He-3 deposits. From the analysis of NASA's satellite gamma ray data, two areas were targeted for possibly holding large concentrations of He-3. Specifically, Mare Tranquillitatis was identified as holding enhanced ilmenite concentrations and other elements that would be essential in any mining mission. The South Pole Aitken basin was also targeted due to its large permanently shadowed areas that enhance its ability to hold volatiles and prevent their migration due to diurnal heating. In general, these results are also consistent with previous lunar site recommendations for locating large He-3 concentrations (e.g. Schmitt, 2006).

SUGGESTIONS FOR FUTURE RESEARCH

Potential areas for further research include investigating

A) current mining technologies and techniques to enhance mining a gas in a low gravity environment;

B) the effects of regolith slope and topography in harvesting solar wind driven He-3;

C) the effects of crustal magnetism on the regolith distribution of He-3; and

D) statistical weighting of He-3 proxies for enhanced He-3 mapping.

Although far from complete, this list identifies research directions with considerable potential for enhancing lunar He-3 exploration as a valuable recourse on the Moon.

REFERENCES CITED

Anand, M., 2010, Lunar Water: A Brief Review: Earth, Moon, and Planets, v. 107.1, p. 65.

Ashley, R.P., Kulcincki, G.L., Santarius, J.F., Krupakar, S.M., Piefer, G., and Radel, R., 2001, Steady-State D 3He Proton Production in an IEC Fusion Device: Fusion Technology-Illinois, v. 39.2, p. 546.

Cho, A., 2009, Helium-3 Shortage Could Put Freeze on Low-Temperature Research: Science, v. 326.5954, p. 778.

Cocks, F.H., 2010, 3He in Permanently Shadowed Lunar Polar Surfaces: Icarus, v. 206.2, p. 778.

Elphic, R.C., Lawrence, D.J., Feldman, W.C., Barraclough, B.L., Gasnault, O.M., Maurice, S., Lucey, P.G., Blewett, D.T., and Binder, A.B., 2002, Lunar Prospector Neutron Spectrometer Constraints on TiO2: Journal of Geophysical Research, v. 107.4.

Fa, W., and Ya-Qiu, J., 2007, Quantitative Estimatino of Helium-3 Spatial Distribution in the Lunar Regolith Layer: Icarus, v. 190.1, p. 15.

Feldman, W.C., Barraclough, B.L., Fuller, K.R., Lawrence, D.J., Maurice, S., Prettyman, T.H., and Binder, A.B., 1999, The Lunar Prospector gamma-ray and neutron spectrometers: Nuclear Instruments and Methods in Physics Research Section A: Accelerators, Spectrometers, Detectors and Associated Equipment, v. 422.1, p. 562.

Feldman, W.C., Maurice, S., Lawrence, D.J., Little, R.C., Lawson, S.L., Gasnault, O.M., Wiens, R.C., Barraclough, B.L., Elphic, R.C., Prettyman, T.H., Steinberg, J.T., and Binder, A.B., 2001, Evidence for Water Ice Near the Lunar Poles: Journal of Geophysical Research, v. 106.10, p. 23231.

Hasebe, N., Shibamura, E., Miyachi, T., Takashima, T., Kobayashi, M., Okudaira, O., Yamashita, N., Kobayashi, S., Ishizaki, T., Sakurai, K., Miyajima, M., Fujii, M., Naraski, K., Takai, S., Tsurumi, K., Kaneko, H., Nakazawa, M., Mori, K., Gasnault, O.M., Maurice, S., d'Uston, C., Reedy, R.C., and Grande, M., 2008, Gamma-ray Spectrometer (GRS) for Lunar Polar Orbiter SELENE: Earth, Moon, and Planets, v. 60.4, p. 299.

Heiken, G., Vaniman, D., and French, B., 1991, Lunar Source Book - A User's Guide to the Moon: Cambridge, Cambridge University.

Johnson, J.R., Swindle, T.D., and Lucey, P.G., 1999, Estimated Solar Wind-implanted Helium-3 Distribution on the Moon: Geographical Research Letters, v. 26.3, p. 385.

Mahdavi, M., and Kaleji, B., 2009, Deutrium/helium-3 Fusion Reactors with Lithium Seeding: Plasma Physics and Controlled Fusion.

Maurice, S., Lawrence, D.J., Feldman, W.C., Elphic, R.C., and Gasnault, O.M., 2004, Reduction of Neutron Data from Lunar Prospector: Journal of Geophysical Research: Planets, v. 109.7.

Nikitin, A., and Bliven, S., 2010, Needs of Well Logging Industry in New Nuclear Detectors: Nuclear Science Symposium Confrence Record (NSS/MIC), IEEE.

O'Reilly, B., and von Frese, R.B.B., Lunar Exploration for He-3, *in* 47th Lunar and Planetary Science Confrence, Houston, p. 1971.

O'Reilly, B., and von Frese, R.B.B., Lunar Exploration for Helium-3, *in* Geologic Society of America, Baltimore.

Pawlowicz, R., 2014, M_Map: A Mapping Package for Matlab

Prettyman, T.H., Feldman, W.C., Lawrence, D.J., Mckinney, G.W., Binder, A.B., Elphic, R.C., Gasnault, O.M., Maurice, S., and Moore, K.R., Library Least Squares Analysis of Lunar Prospector Gamma-ray Spectra, *in* 33rd Lunar and Planetary Science Conference, Houston, p. 2012.

Ribeiro, R.A.P., and de Lazaro, S.R., 2014, Structural, Electronic and Elastic Properties of FeBO3 (B=Ti, Sn, Si, Zr) Ilmenite: A Density Functional Theory Study: RSC Advences, v. 4.104, p. 59839.

Schmitt, H.H., 2006, Resources: Lunar Helium-3 Economics, *in* Return to the Moon: Ecploration, Enterprise, and Energy in the Human Settlement of Space.

Schmitt, H.H., Kulcincky, G.L., Santarius, J.F., Ding, J., Malecki, M.J., and Zalewski, M.J., 2000, Solar-Wind Hydrogen at the Lunar Poles: Constratints on the Volatile Distribution within Shackleton Crater at the Lunar South Pole, p. 653.

Shea, D.A., and Morgan, D., 2010, The Helium-3 Shortage: Supply, Demand, and Options for Congress: Congressional Research Service.

Vasavada, A.R., Paige, D.A., and Wood, S.E., 1999, Near Surface Temperatures on Mercury and the Moon and the Stability of Polar Ice Deposits: Icarus, v. 141, p. 179.

Wang, Z., Li, Y., Jiang, J., and Li, D., 2010, Lunar Surface Dielectric Constant, Regolith Thickness, and 3He Abundance Distributions Retrieved from the Microwave Brightness Temperatures of CE-1 Lunar Microwave Sounder: Science China Earth Sciences, v. 53.9, p. 1365.

Zuber, M.T., Head, J.W., Smith, D.E., Neuman, G.A., Mazarico, E., Torrence, M.H., Aharonson, O., Tye, A.R., Fassett, C.I., Rosenburg, M.A., and Melosh, H.J., 2012, Constraints on the Volatile Distribution within Shackleton Crater at the Lunar South Pole: Nature, v. 486.7403, p. 378.

APPENDIX A

```
function timap(LonMax,LatMax,Ti)
m_proj('sinusoidal','longitudes',[-90 90],'latitudes',[-65 65]);
m_grid
[x,y]=meshgrid(-90:1:90,-65:1:65);
[X,Y]=m_ll2xy(x,y);
%they are L's not 1's
dem=griddata(LonMax,LatMax,Ti,x,y);
hold on
contourf(X,Y,dem)
figure
m_proj('sinusoidal','longitudes',[90 270],'latitudes',[-65 65]);
m_grid
[xf,yf]=meshgrid(90:1:180,-65:1:65);
[xf1,yf1]=meshgrid(-180:1:-90,-65:1:65);
[xfx,yfy]=meshgrid(180:1:270,-65:1:65);
[Xf,Yf]=m_ll2xy(xf,yf);
[Xf1,Yf1]=m_ll2xy(xfx,yfy);
demf=griddata(LonMax,LatMax,Ti,xf,yf);
demf1=griddata(LonMax,LatMax,Ti,xf1,yf1);
hold on
contourf(Xf,Yf,demf)
contourf(Xf1,Yf1,demf1)
end
```

Figure A1. MATLAB script used to produce elemental concentration maps of the lunar near and far sides. This specific example shows the script for plotting the Ti maps in Figure 3.

```
function hmap(lonMax,latMax,H)
m_proj('sinusoidal','longitudes',[-90 90],'latitudes',[-65 65]);
m_grid
[x,y]=meshgrid(-90:1:90,-65:1:65);
[X,Y]=m_ll2xy(x,y);
%they are L's not 1's
dem=griddata(lonMax,latMax,H,x,y);
hold on
contourf(X,Y,dem)
figure
m_proj('sinusoidal','longitudes',[90 270],'latitudes',[-65 65]);
m_grid
[xf,yf]=meshgrid(90:1:180,-65:1:65);
[xf1,yf1]=meshgrid(-180:1:-90,-65:1:65);
[xfx,yfy]=meshgrid(180:1:270,-65:1:65);
[Xf,Yf]=m_ll2xy(xf,yf);
[Xf1,Yf1]=m_ll2xy(xfx,yfy);
demf=griddata(lonMax,latMax,H,xf,yf);
demf1=griddata(lonMax,latMax,H,xf1,yf1);
hold on
contourf(Xf,Yf,demf)
contourf(Xf1,Yf1,demf1)
figure
m_proj('stereographic','lat',90,'long',30,'radius',25);
m_grid
hold on
[xn1,yn1]=meshgrid(-90:1:90,65:1:90);
[Xn1,Yn1]=m_ll2xy(xn1,yn1);
demn1=griddata(lonMax,latMax,H,xn1,yn1);
contourf(Xn1,Yn1,demn1)
[xn2,yn2]=meshgrid(90:1:180,65:1:90);
[Xn2,Yn2]=m_ll2xy(xn2,yn2);
demn2=griddata(lonMax,latMax,H,xn2,yn2);
contourf(Xn2,Yn2,demn2);
[xn3,yn3]=meshgrid(180:1:270,65:1:90);
[Xn3,Yn3]=m_ll2xy(xn3,yn3);
demn3=griddata(lonMax,latMax,H,xn3,yn3);
contourf(Xn3,Yn3,demn3);
[xn4,yn4]=meshgrid(-180:1:-90,65:1:90);
[Xn4,Yn4]=m_ll2xy(xn4,yn4);
demn4=griddata(lonMax,latMax,H,xn4,yn4);
contourf(Xn4,Yn4,demn4);
figure
m_proj('stereographic','lat',-90,'long',-30,'radius',25);
m_grid('xaxislocation','top')
hold on
[xs1,ys1]=meshgrid(-90:1:90,-90:1:-65);
[Xs1,Ys1]=m_ll2xy(xs1,ys1);
dems1=griddata(lonMax,latMax,H,xs1,ys1);
contourf(Xs1,Ys1,dems1)
[xs2,ys2]=meshgrid(90:1:180,-90:1:-65);
[Xs2,Ys2]=m_ll2xy(xs2,ys2);
dems2=griddata(lonMax,latMax,H,xs2,ys2);
contourf(Xs2,Ys2,dems2);
[xs3,ys3]=meshgrid(180:1:270,-90:1:-65);
[Xs3,Ys3]=m_ll2xy(xs3,ys3);
dems3=griddata(lonMax,latMax,H,xs3,ys3);
contourf(Xs3,Ys3,dems3);
[xs4,ys4]=meshgrid(-180:1:-90,-90:1:-65);
[Xs4,Ys4]=m_ll2xy(xs4,ys4);
dems4=griddata(lonMax,latMax,H,xs4,ys4);
contourf(Xs4,Ys4,dems4);
end
```

Figure A2. MATLAB script used to produce elemental concentration maps on the lunar near and far sides, and the polar regions. This specific example shows the script for plotting the H maps in Figure 4.

```
if (pi*(.25)) >=abs(lonr);
    delta=2+sin(lonr-f*pi)-sin(lonr+f*pi);

elseif (abs(lonr))<=(pi*(.75));
    delta=1+sin(abs(lonr)-f*pi);

else
    delta=2;
end;
```

Figure A3. MATLAB script used to implement Equation 1 for the average solar wind flux exposure over a single lunar orbital period.

APPENDIX B

Thesis Defense Slides

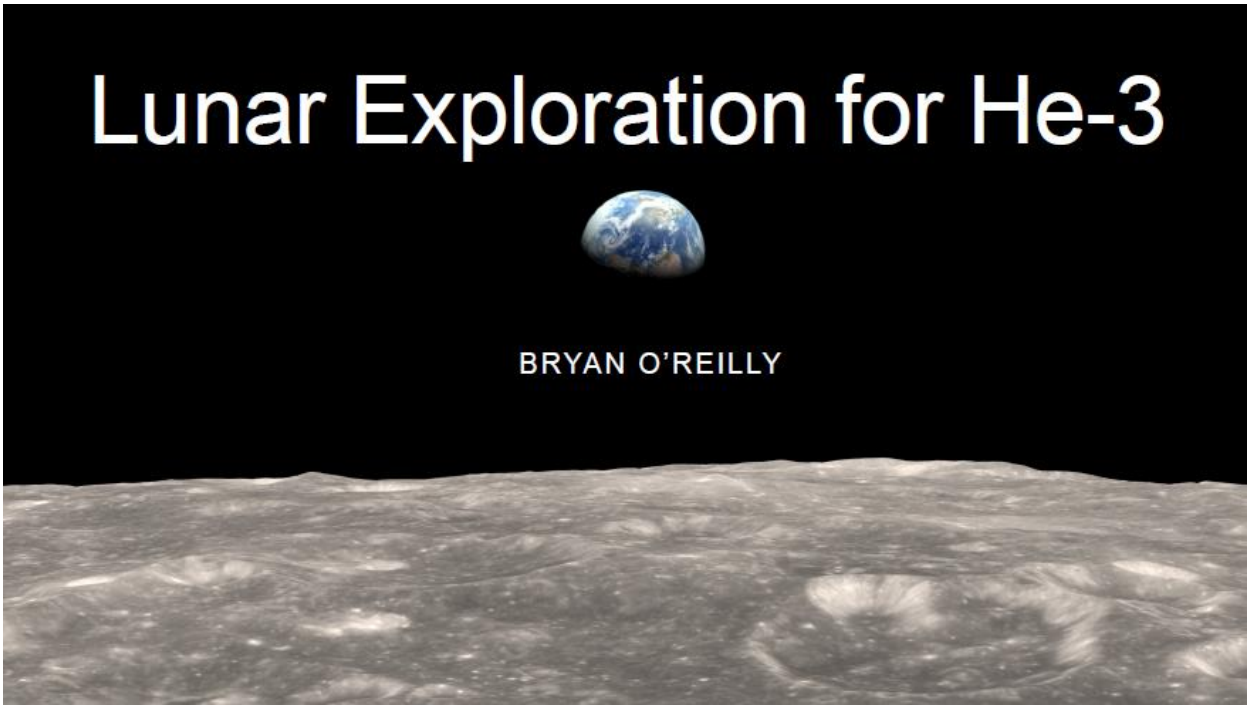

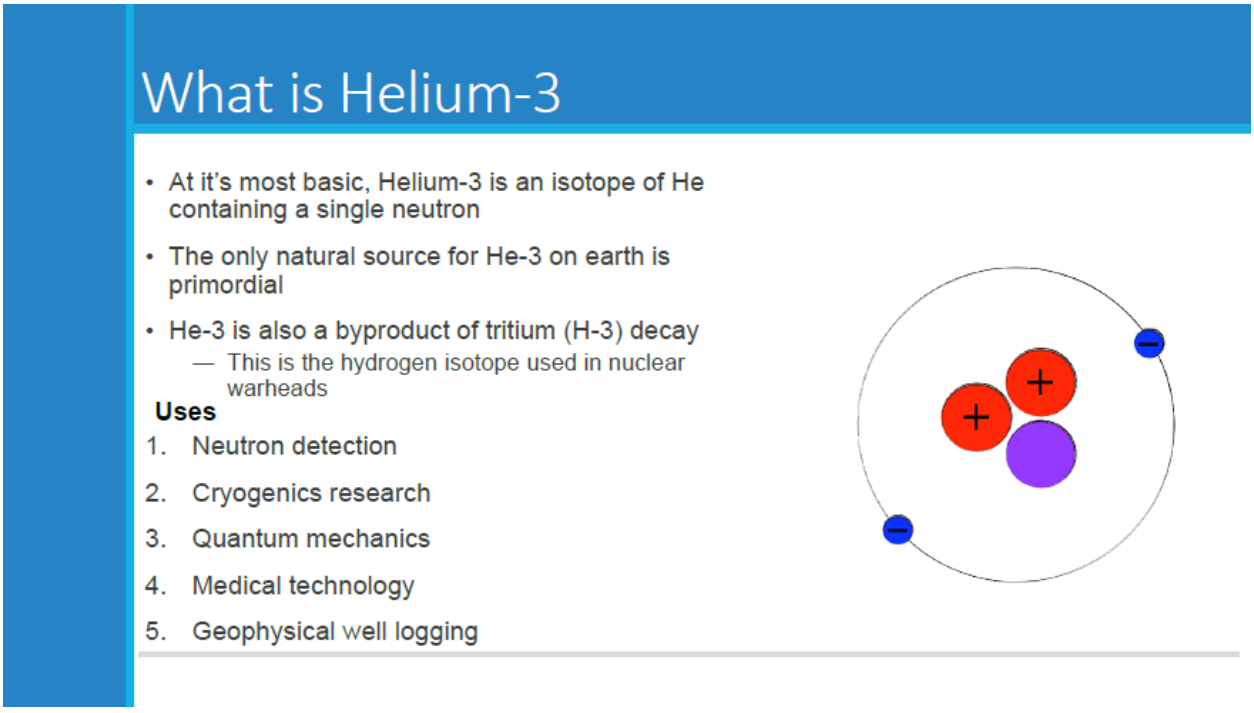

The Shortage

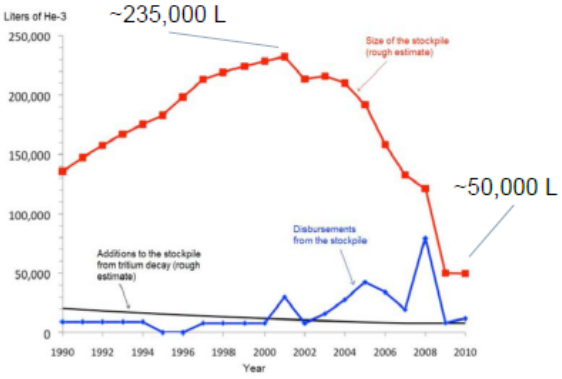

(Shea and Morgan, 2010)

- Demand began to increase in 2001 following 9/11
- From 2001 to 2010 the price of He-3 increased from $200/L to $2,000/L
- Decrease in the U.S. nuclear weapons stockpile through arms agreements

Objectives

- Identify factors associated with large concentrations of He-3 on the lunar surface
- Examine how lunar surface geology influences these concentrations
- Gain an understanding of how He-3 is deposited within the lunar surface
- Use NASA satellite data to support these claims
- Identify areas of large He-3 concentrations

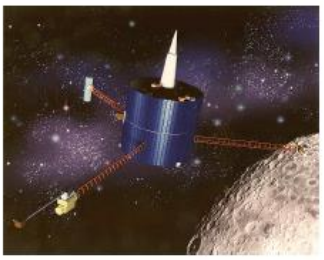

(Lunar Planetary Institute)

Proxies for Lunar He-3

1. Solar wind exposure
   - He-3 is transported to the moon through solar wind
2. Titanium distribution
   - Lunar Ti is associated with higher He-3 concentrations
3. Diurnal temperature shifts
   - Extreme temperature shifts reduce He-3 in non-polar regions
4. Polar migration of volatiles
   - Despite lack of solar wind exposure there are high concentrations of volatiles present around the lunar poles

The Regolith

- Regolith is the uppermost layer, covering the entirety of the lunar surface
- Around 5 or 6 meters thick in the maria and on average 10 meters in the highlands
- Consists of fragmental material broken up by constant impacts

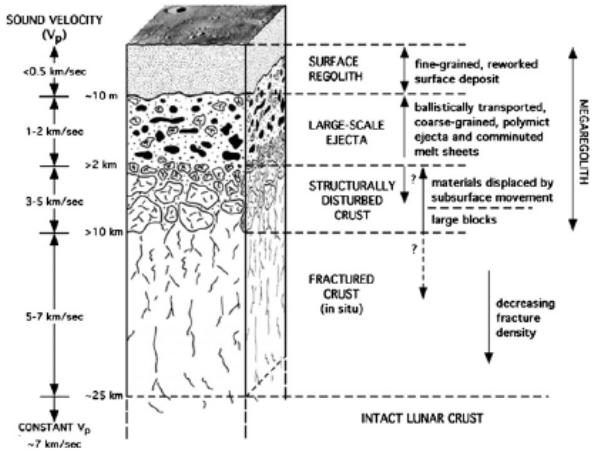

(Wilhelms et al., 1987)

Lunar He-3 Deposition

- He-3 forms, along with other volatiles, within the sun and is pushed outward as energized solar wind
- The wind interacts with the earth magnetosphere creating a bow shape
- The moon lacks a magnetosphere so it is unprotected
  - This allows particles in the solar wind to deposit within the regolith

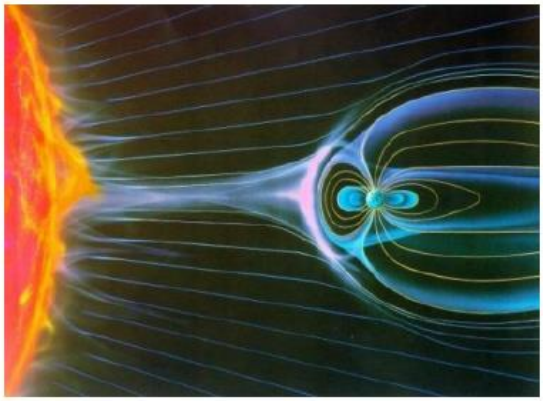

(NASA)

The Phases of The Moon

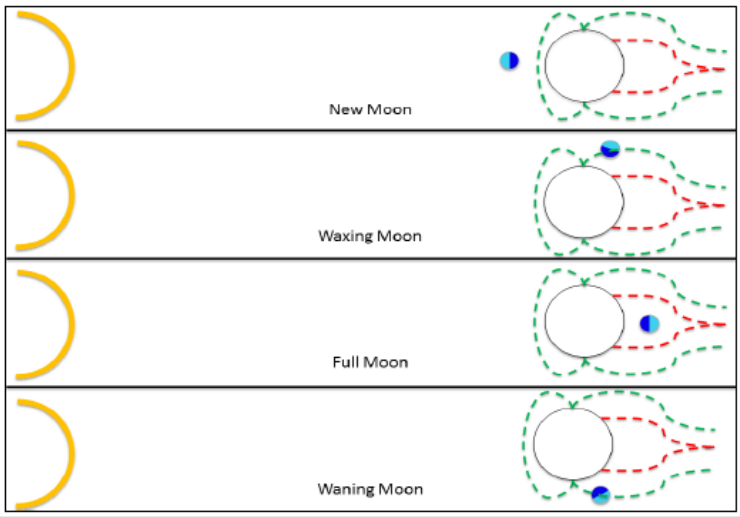

Legend	
Light Blue	Lunar Farside
Dark Blue	Lunar Nearside
Yellow	Sun
Green Line	Magnetosphere
Red Line	Magnetotail

Solar Wind Exposure

The equation below was used to calculate the normalized solar wind exposure on the lunar surface

$$F(\Phi,\theta) = F_0 cos(\Phi) * \begin{cases} 2 + sin(\theta - f\pi) - sin(\theta + f\pi), |\theta| \le \pi(.5 - f) \\ 1 + sin(|\theta| - f\pi), \pi(0.5 - f) \le |\theta| \le \pi(.5 + f) \\ 2, \pi(.5 + f) \le |\theta| \le \pi \end{cases}$$

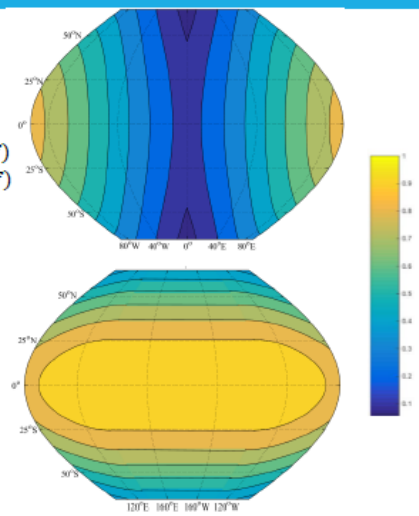

In the equation:

- Φ = Latitude
- θ = Longitude
- F_0 = 0.5
  - constant subsolar wind exposure
- f = 0.25
  - The percent of time the moon is fully shielded

Titanium Distribution

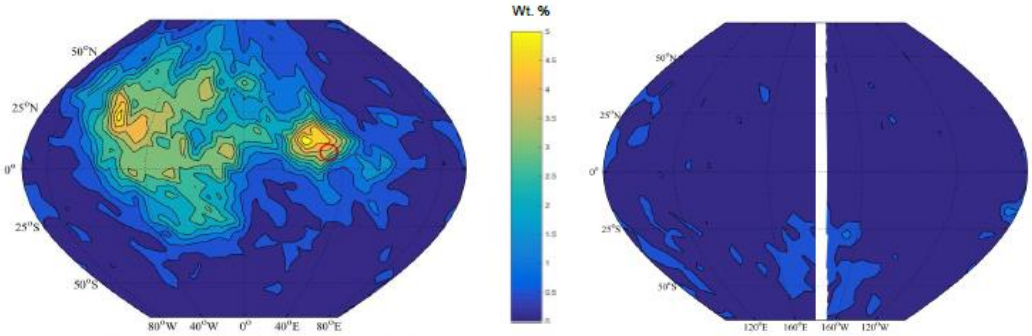

- Lunar Ti appears in the form of Ilmenite
- Ilmenite typically forms as a result of large impact events
- The materials introduced by the asteroid and the pressure and temperature increases from the impact event cause basaltic melting

Ilmenite

- Lunar Ilmenite ($FeTiO_3$) is associated with higher He-3 concentrations
- It has a Triagonal (Rhombohedral) crystal system
- Alternating layers of Ti and Fe with O situated in between
- The structure of Ilmenite may create a more sustainable trap for the He-3

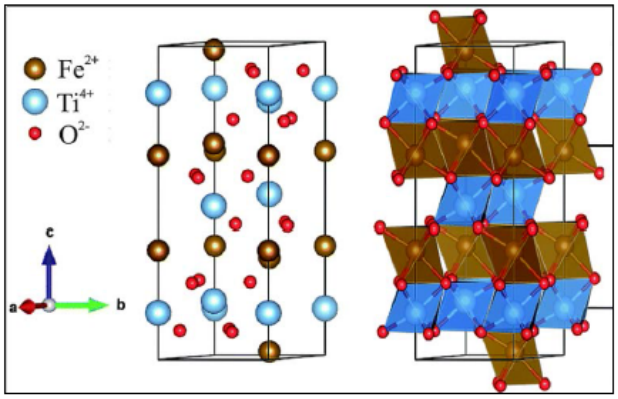

(Ribeiro and Lazaro, 2014)

Diurnal Temperature Shifts

- Subpolar latitudes (±60˚) experience intense shifts in temperature throughout a lunar orbital period
- These subpolar regions on average undergo a change of around 285˚K
  - From 375˚K to 90˚K
- The large temperature shifts can cause volatiles "baked out" of the regolith
  - Once reionized the volatile isotopes leave the regolith back into space
  - Some of the isotopes released are deposited elsewhere on the lunar surface
- Polar regions tend to stay around 115˚K fluctuating ~10˚K in a given orbital period
  - Prevents reionization

Permanently Shadowed Craters

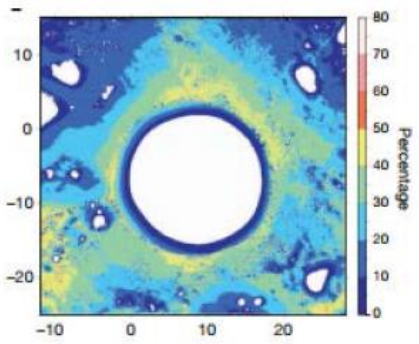

(Zuber et al., 2012)

- Permanently shadowed craters located in the polar regions undergo the smallest temperature shifts on the lunar surface
- The lack of illumination along the rims of these craters protects volatiles from reionization
- The rims of the permanently shadowed craters also protect from micrometeoroid impacts
- The Shackleton crater, located in the South Pole – Aitken basin, is an example of one of these craters

Polar Migration of Volatiles

- H, like He-3, is a product of solar wind exposure
- With the amount of exposure the lunar farside experiences, large concentrations of H might be expected
- The largest concentrations appear to be around the poles where there is minimal exposure

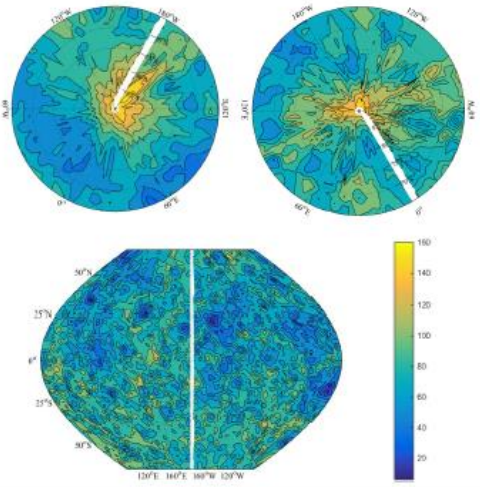

Locations for Investigation

2 main areas for further investigation

Mare Tranquillitatis

- Due to high Ti concentrations this location may be able to sustain high concentrations of He-3

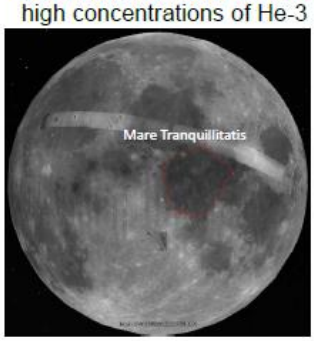

(Google Earth)

South Pole – Aitken Basin

- Large permanently shadowed craters offer protection from extreme temperature fluctuations

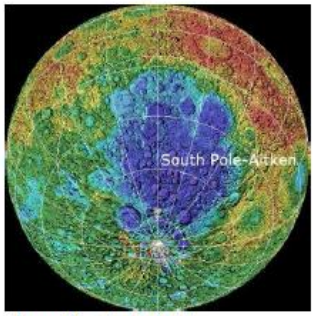

(Lunar Planetary Institute)

Conclusion

- He-3 is initially deposited within the lunar surface through exposure to solar winds
  - Due to the Earth's magnetosphere, a majority of this exposure occurs on the lunar farside
- Most of the He-3 initially deposited is reionized due to diurnal temperature shifts
  - The He-3 is then either released or redeposited elsewhere on the lunar surface
- Maria on the lunar nearside are able to sustain He-3 concentrations despite these temperature shifts
  - This is due to high concentrations of Ilmenite located in these craters
- The polar regions are also able to sustain high concentrations of volatiles
  - Due to the fact that these regions do not experience the same diurnal heating patterns
  - The presence of permanently shadowed craters
- There are two areas of interest for further study based on these factors
  - Mare Tranquillitatis
  - The South Pole – Aitken Basin

Acknowledgments

- I would like to thank Dr. Ralph von Frese for his advice and guidance over the course of my research
- Dr. Hyung Rae Kim for the valuable Matlab training
- Dr. Anne Carey for her work with the SURE program
- The OSU Division of Natural and Mathematical Sciences for the Mayers Summer Research Scholarship
- Shell Exploration and Production Company for partial funding of this research
- NASA provided a large portion of the instrumental data used in this study

Work cited

Cho, Adrian, "Helium-3 Shortage Could Put Freeze on Low-Temperature Research," Science, November 6, 2009, pp. 778-779.

Cocks, Franklin Hadley. "3 He in permanently shadowed lunar polar surfaces." Icarus 206.2 (2010): 778-779.

Fa, Wenzhe, and Ya-Qiu Jin. "Quantitative Estimation of Helium-3 Spatial Distribution in the Lunar Regolith Layer." *Icarus* 190.1 (2007): 15-23.

Feldman, W. C., et al. "The Lunar Prospector gamma-ray and neutron spectrometers." *Nuclear Instruments and Methods in Physics Research Section A: Accelerators, Spectrometers, Detectors and Associated Equipment* 422.1 (1999): 562-566.

Heiken, G., Vaniman, D., French, B., 1991. Lunar Source Book – A User's Guide to the Moon. Cambridge University, Cambridge. p. 34.

Johnson, Jeffrey R., Timothy D. Swindle, and Paul G. Lucey. "Estimated Solar Wind-implanted Helium-3 Distribution on the Moon." *Geophysical Research Letters* 26.3 (1999): 385.

Lunar and Planetary Institute. The Lunar Prospector Mission, Image of the Lunar Prospector.

Lunar and Planetary Institute. Clementine Altimeter Data, South Pole – Aitken Basin.

Maurice, S., et al. "Reduction of neutron data from Lunar Prospector." *Journal of Geophysical Research: Planets* 109.E7 (2004).

Ribeiro, R. A. P., and S. R. de Lazaro. "Structural, electronic and elastic properties of FeBO 3 (B= Ti, Sn, Si, Zr) ilmenite: a density functional theory study." RSC Advances 4.104 (2014): 59839-59846.

Sahraoui, F., Goldstein, M.L., Robert, P., Khotyaintsev, Y.V., *Evidence of cascade and dissipation of solar wind turbulence at electrons scales*, Physical Review Letters, 02, 231102 (2009). DOI: 10.1103/PhysRevLett.102.231102

Schmitt, Harrison H. "Resources: Lunar Helium-3 Economics." Return to the Moon: Exploration, Enterprise, and Energy in the Human Settlement of Space (2006): 77-108.

Shea, Dana A., and Daniel Morgan. "The helium-3 shortage: Supply, demand, and options for Congress." Congressional Research Service, Library of Congress, 2010.

Wilhelms, Don E., F. John, and Newell J. Trask. *The geologic history of the Moon*. No. 1348. 1987.

Zuber, Maria T., et al. "Constraints on the volatile distribution within Shackleton crater at the lunar south pole." Nature 486.7403 (2012): 378-381.